



### **Heavily Doped Semiconductor Nanocrystal Quantum Dots**

David Mocatta, et al. Science **332**, 77 (2011); DOI: 10.1126/science.1196321

This copy is for your personal, non-commercial use only.

If you wish to distribute this article to others, you can order high-quality copies for your colleagues, clients, or customers by clicking here.

**Permission to republish or repurpose articles or portions of articles** can be obtained by following the guidelines here.

The following resources related to this article are available online at www.sciencemag.org (this infomation is current as of April 5, 2011):

**Updated information and services,** including high-resolution figures, can be found in the online version of this article at:

http://www.sciencemag.org/content/332/6025/77.full.html

Supporting Online Material can be found at:

http://www.sciencemag.org/content/suppl/2011/03/31/332.6025.77.DC1.html http://www.sciencemag.org/content/suppl/2011/03/31/332.6025.77.DC2.html

A list of selected additional articles on the Science Web sites **related to this article** can be found at:

http://www.sciencemag.org/content/332/6025/77.full.html#related

This article **cites 28 articles**, 5 of which can be accessed free: http://www.sciencemag.org/content/332/6025/77.full.html#ref-list-1

This article has been **cited by** 1 articles hosted by HighWire Press; see: http://www.sciencemag.org/content/332/6025/77.full.html#related-urls

This article appears in the following **subject collections**: Materials Science

http://www.sciencemag.org/cgi/collection/mat\_sci

- D. R. Link, N. Chattham, J. E. Maclennan, N. A. Clark, Phys. Rev. E Stat. Nonlin. Soft Matter Phys. 71, 021704 (2005).
- P. M. Johnson, S. Pankratz, P. Mach, H. T. Nguyen,
  C. C. Huang, *Phys. Rev. Lett.* 83, 4073 (1999).
- 25. M. Nakata et al., Liq. Cryst. 28, 1301 (2001).
- N. A. Clark, D. Coleman, J. E. Maclennan, Liq. Cryst. 27, 985 (2000).
- M. J. O'Callaghan, M. D. Wand, C. M. Walker, M. Nakata, *Appl. Phys. Lett.* 85, 6344 (2004).
- 28. L. Radzihovsky, P. B. Weichman, J. I. Park, *Ann. Phys.* **323**, 2376 (2008).
- 29. D. M. Walba et al., Science 288, 2181 (2000).
- 30. This work was supported by NSF Materials Research Science and Engineering Center grant DMR 0820579, NSF grant DMR 0606528, NSF grant DMR 0603223, and NASA grant NAG-NNC04GA50G. Use of the National Synchrotron Light Source was supported by the U.S. Department of Energy, Divisions of Materials and Chemical Sciences.

#### Supporting Online Material

www.sciencemag.org/cgi/content/full/332/6025/72/DC1 Materials and Methods SOM Text Figs. S1 to S9 References

2 September 2010; accepted 15 February 2011 10.1126/science.1197248

## Heavily Doped Semiconductor Nanocrystal Quantum Dots

David Mocatta, <sup>1,2</sup> Guy Cohen, <sup>3</sup> Jonathan Schattner, <sup>2,4</sup> Oded Millo, <sup>2,4</sup>\* Eran Rabani, <sup>3</sup>\* Uri Banin <sup>1,2</sup>\*

Doping of semiconductors by impurity atoms enabled their widespread technological application in microelectronics and optoelectronics. However, doping has proven elusive for strongly confined colloidal semiconductor nanocrystals because of the synthetic challenge of how to introduce single impurities, as well as a lack of fundamental understanding of this heavily doped limit under strong quantum confinement. We developed a method to dope semiconductor nanocrystals with metal impurities, enabling control of the band gap and Fermi energy. A combination of optical measurements, scanning tunneling spectroscopy, and theory revealed the emergence of a confined impurity band and band-tailing. Our method yields n- and p-doped semiconductor nanocrystals, which have potential applications in solar cells, thin-film transistors, and optoelectronic devices.

oping of bulk semiconductors, the process of intentional insertion of impurity atoms into a crystal, was introduced in the 1940s and is the basis for the widespread application of semiconductors in electronic and electro-optic components (1). Controlling the size and dimensionality of semiconductor structures is an additional way to tune their properties via quantum confinement effects. In this respect, colloidal semiconductor nanocrystals (NCs) have emerged as a family of materials with size-dependent optical and electronic properties. Combined with their capability for wet-chemical processing, this has led to NC-based light-emitting diodes (2), solar cells, (3) and transistor devices (4) prepared via facile and scalable bottom-up approaches. Impurity doping in such colloidal NCs still remains a challenge (5). From the synthesis side, the introduction of a few impurity atoms into a NC that contains only a few hundred atoms may lead to their expulsion to the surface (6–8) or compromise the crystal structure. This will inherently create a heavily doped NC under strong quantum confinement. The electronic and optical properties in such circumstances are still unresolved.

Several strategies for NC doping have been used. Remote doping, through the use of binding ligands on the nanoparticle surface (which can donate carriers) or electrochemical carrier

injection, has been shown to yield n-type doping in semiconductor NC superlattices (4, 9–11). Substitutional doping has been studied mainly for color center impurities (12) and magnetic impurities, notably Mn atoms (13, 14), thereby providing insight into the challenging chemistry (15). The introduction of dopant precursors at specific stages of nanoparticle growth has been effective in controlling the impurity location (16). More recently, some progress has been made toward producing n-type CdSe quantum dots (QDs) through the use of tin and indium impurities (17, 18), and Cu impurities have been used to produce p-type InP NCs (19).

Here, we describe a simple room-temperature method for doping semiconductor NCs with metal impurities. By changing the dopant type and concentration, we achieved exquisite control of the electronic properties, including the band gap and Fermi energy. We conducted experimental and theoretical studies of the role of strong quantum confinement leading to localization of the impurity wave functions as well as disorder effects

Scattered

Impurities

 $^{1S}_{r}$  band

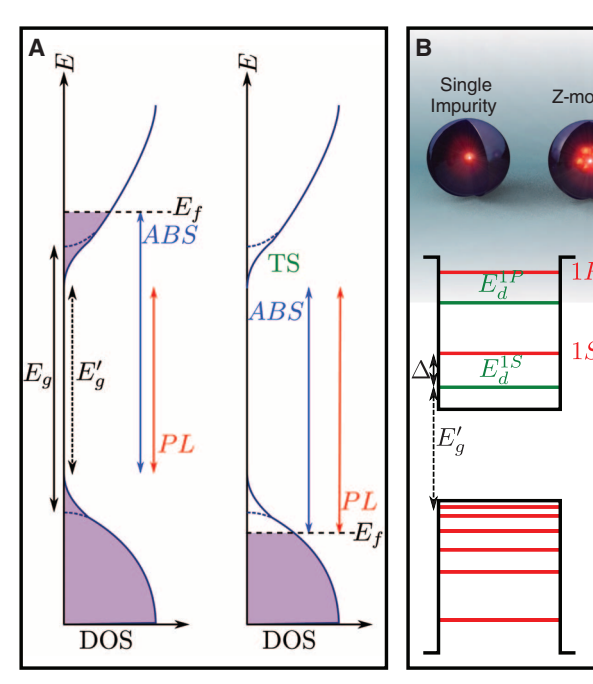


**Fig. 1.** Diagrams describing the effects of heavy doping in bulk and nanocrystal semiconductors. (**A**) Scheme of the different influences of doping a bulk semiconductor for n-type (left) and p-type (right) dopants. ABS, absorption onset; PL, photoluminescence onset; TS, tail states;  $E_f$ , Fermi energy;  $E'_g$ , modified band gap;  $E_g$ , unperturbed band gap. The purple shading shows state filling up to the Fermi energy. (**B**) Sketch for n-doped nanocrystal QD with confined energy levels. Red and green lines correspond to the QD and impurity levels, respectively. Left panel: The level diagram for a single impurity effective mass model, where  $E'_g$  is the quasi-particle gap in the doped QD,  $1S_e$  and  $1P_e$  are the QD electron levels, and  $E_d^{1S}$  and  $E_d^{1P}$  are the impurity levels shifted below the corresponding QD levels by a shift  $\Delta$ . Right panel: Impurity levels develop into impurity bands as the number of impurities increases. Upper panel: Sketch of the different impurity models.

<sup>&</sup>lt;sup>1</sup>Institute of Chemistry, Hebrew University, Jerusalem 91904, Israel. <sup>2</sup>Center for Nanoscience and Nanotechnology, Hebrew University, Jerusalem 91904, Israel. <sup>3</sup>School of Chemistry, Sackler Faculty of Exact Sciences, Tel Aviv University, Tel Aviv 69978, Israel. <sup>4</sup>Racah Institute of Physics, Hebrew University, Jerusalem 91904, Israel.

<sup>\*</sup>To whom correspondence should be addressed. E-mail: uri.banin@huji.ac.il (U.B.); rabani@tau.ac.il (E.R.); milode@vms.huji.ac.il (O.M.)

leading to band-tailing in small NCs. The method yields n- and p-doped semiconductor NCs that greatly enhance the usefulness of such materials in solar cells, thin-film transistors, and optoelectronic devices.

Adding even a single impurity atom to a semiconductor NC with a diameter of 4 nm, which contains about 1000 atoms, leads to a nominal doping level of  $7 \times 10^{19}$  cm<sup>-3</sup>. In a bulk semiconductor this is already well within the heavily doped limit, where metallic ("degenerate") behavior is expected (20). Heavy doping in bulk semiconductors leads to several effects summarized in Fig. 1A. The impurities interact with each other and an impurity subband emerges near the edge of the respective band (conduction or valence for n- or p-type, respectively). Indeed, this is the criterion that defines the heavily doped regime. Often, tail states (Urbach tails) also develop as a result of distortions in the crystal structure (21). In effect, the band gap  $E_{\sigma}$  is narrowed. This may be probed by optical means, where for heavily doped n-type semiconductors (Fig. 1A, left frame) the absorption is blue-shifted as a result of conduction band-filling by the donated electrons (Moss-Burstein effect) (20), and the emission emanating from the bottom of the conduction band is red-shifted. For heavy p-type doping, both absorption and emission are typically seen to be red-shifted. This is due to the high density of states (DOS) near the valence band edge, leading to a small Moss-Burstein effect that is often overcome by the red shift due to band-tailing (20).

A markedly different situation arises for impurity doping of NCs because of the discrete nature of the quantum-confined states (shown for n-type doping in Fig. 1B). In this case the addition of a single dopant (left frame) introduces impurity levels that significantly alter the DOSa situation that is not expected for prior remote surface doping strategies. This has been described by a hydrogenic model under spherical confinement, leading to S- and P-like impurity states denoted by  $E_{\rm d}^{1S}$  and  $E_{\rm d}^{2P}$  that are several tens of meVs below the corresponding dot levels, effectively doubling the DOS near those energies (22-24). Even more intriguing is the case introduced here, of multiple impurities in a single dot, which are inherently interacting because of the small volume and experience the effect of the confining potential (Fig. 1B, right frame). In this heavily doped regime, the nature of delocalization and interaction of the impurity charge carriers may be greatly modified relative to the bulk case. In addition, multiple impurities in a small confined NC can enhance disorder effects, altering the electronic structure via a quantumconfined Urbach tail mechanism.

To dope InAs NCs with different impurity atoms, we modified a reaction used for gold growth onto semiconductor nanoparticles, which demonstrated the ability to introduce Au into InAs NCs by diffusion (25). In a typical metal atom–doping synthesis, the metal salt (CuCl<sub>2</sub>, AgNO<sub>3</sub>, AgCl, or AuCl<sub>3</sub>) is dissolved in a tol-

uene solution with appropriate surfactant and gradually added to a solution of preformed InAs NCs in toluene at room temperature (26). The use of preformed NCs allows changes to the properties of the NCs to be assigned wholly to the introduction of the impurity atoms. In general, previous doping methods are based on impurity introduction during NC synthesis, and hence assigning changes to the NC properties are complicated by the inability to differentiate between the influence of the impurity on the NC and the influence of the impurity precursor on the synthesis. This well-controlled approach allows us to follow the intricate changes in the NC properties upon introduction of dopants.

Figure 2A shows a transmission electron microscope (TEM) image of Ag-doped NCs. At the impurity levels reported below, it was not possible to identify the presence of metal regions, indicating that the impurity atoms are dispersed (fig. S8). This was not the case for very high metal atom concentrations (>3000 atoms per NC in the reaction solution), where TEM analysis clearly showed phase separation between InAs and impurity metal regions (25). Further support for the dispersion of impurities is provided by x-ray diffraction (fig. S10), where no fingerprints of metal domains were detected while the InAs crystal structure was generally maintained. Some broadening of the peaks is seen, ascribed to a small degree of structural disorder. X-ray photoelectron spectroscopy (XPS) measurements of these samples were also performed, indicating the presence of Ag, Au, and Cu in the respective samples (figs. S11 and S12). This suggests successful addition of these atoms to the InAs NCs, consistent with our previous report of Au growth on InAs NCs, which exhibited the room-temperature solid-state diffusion of Au into the NC (25). Indeed, extrapolating the diffusion parameter values to room temperature gives a diffusion length scale of  $\sim 10^4$  nm per 24 hours, far greater than the NC diameter; large values are also extrapolated for Ag and Cu (table S1).

Figure 2B shows the absorption and emission (inset) spectra of undoped and doped InAs NCs. The addition of Ag atoms results in a red shift of both the first exciton absorption and the emission peaks. The addition of Cu results in a blue shift of the first exciton absorption peak, whereas the emission is not shifted. Addition of Au at similar concentrations does not considerably alter the observed optical gap either in absorption or in emission. The addition of any of these impurity atoms results in the gradual quenching of the emission from the NCs, yet the three impurities lead to qualitatively different effects on the optical spectra and hence on the electronic properties of the doped NCs. The effect of varying amounts of impurities on the first absorption peak and on the emission is shown in Fig. 2, C to E, for InAs NCs with different diameters (see figs.

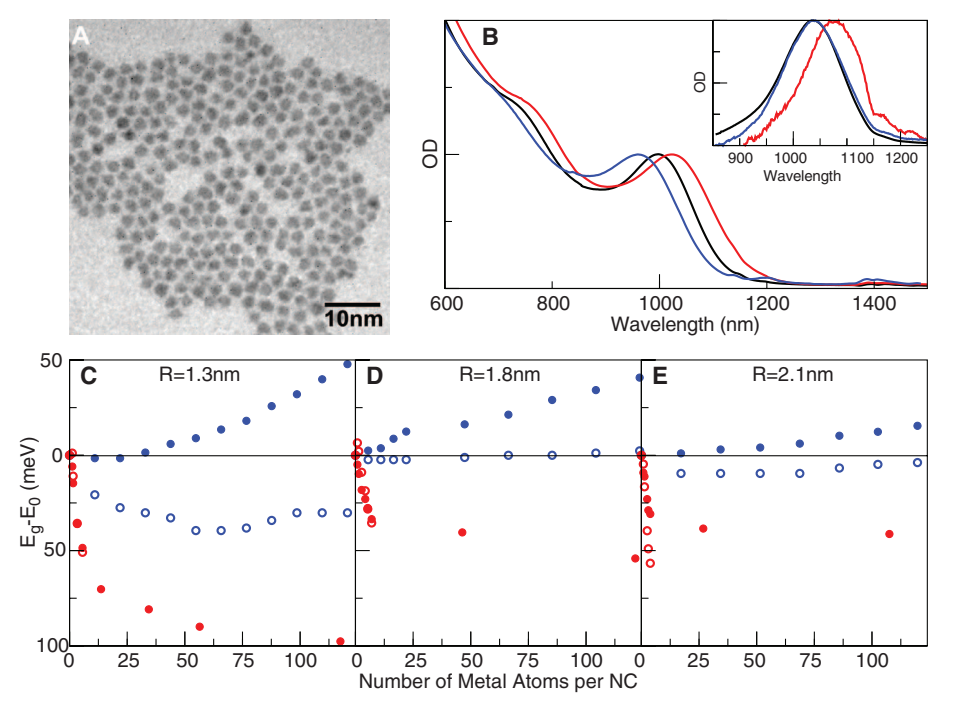


**Fig. 2.** Optical properties of doped InAs NCs. (**A**) TEM image of Ag-doped 3.3-nm InAs NCs. (**B**) Normalized absorption spectra of three 3.3-nm InAs NC samples. Two of the samples had Cu (blue) and Ag (red) solutions added to them resulting in metal/NC solution ratios of 540 and 264, respectively. These amounts correspond to 73 Cu atoms and 9 Ag atoms per NC. The third sample had a control solution (without metal salt) added to it (black). The inset shows the normalized emission spectra of these samples. (**C** to **E**) The energetic shift of the first exciton peak (solid symbols) and the emission energy (open symbols) against the number of impurity atoms per QD for InAs NCs with radii of 1.3 nm (C), 1.8 nm (D), and 2.1 nm (E). Red symbols correspond to Ag doping, blue symbols to Cu.

S1 and S2 for individual spectra). No considerable bleaching effects were observed in the absorption. The amount of impurities on the NCs was estimated by the analytical method of inductively coupled plasma atomic emission spectroscopy (ICP-AES, figs. S3 to S7).

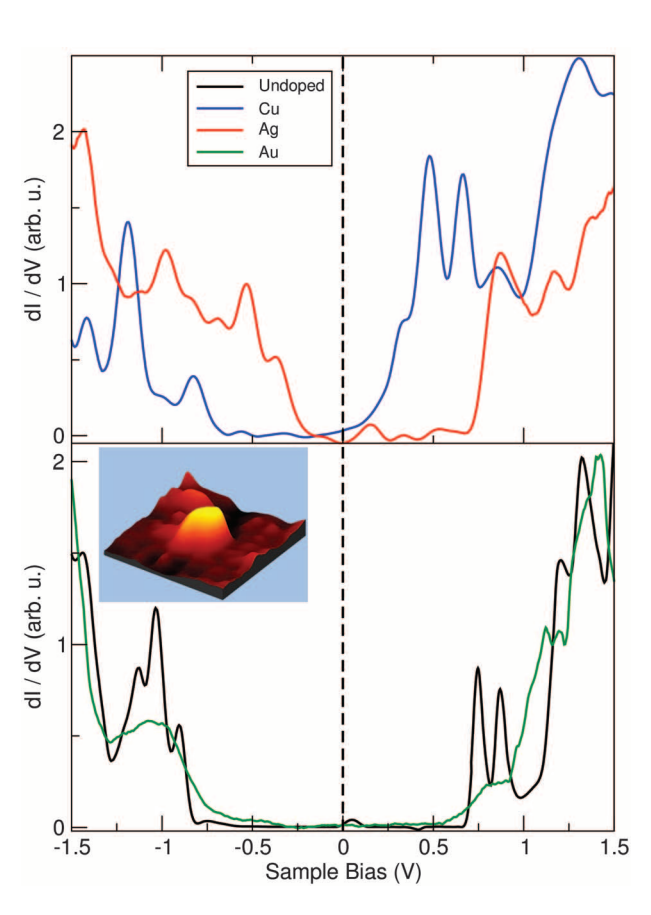
A first possible source of spectral shifts in such quantum confined particles may be related to size changes upon doping, but this was excluded by detailed sizing analysis (fig. S9). An alternative source of the spectral shifts can be associated with electronic doping by the impurities. In Fig. 3 we show tunneling spectra measured by a scanning tunneling microscope (STM) at T = 4.2 K for undoped, Au-doped, Cu-doped, and Ag-doped InAs QDs 4.2 nm in diameter (see figs. S13 to S15 for additional spectra). Starting from the reference case of the undoped QD shown in the lower panel, the dI/dV curves, which are proportional to the DOS, match earlier studies of InAs ODs (27). The gap region is clearly identified, whereas on the positive-bias side a doublet of peaks associated with tunneling through the doubly degenerate 1Se state is seen at the onset of the current, followed by a higher-order multiplet at higher bias corresponding to tunneling through the  $1P_e$  conduction band state. A more complex peak structure is seen on the negative-bias side, resulting from tunneling through the closely spaced and intricate valence band states.

Several changes are seen upon doping the QDs. Starting with the case of Au, the gap is

Fig. 3. The effect of doping on the STM tunneling spectra. Four dl/dV versus V tunneling spectra at 4.2 K, of undoped (black trace), Au-doped (green trace), Cu-doped (blue trace), and Ag-doped (red trace) InAs nanocrystals, nominally 4 nm in diameter. The doped QDs were taken from samples that had Ag, Cu, and Au atom/QD ratios corresponding to 15, 160, and 77, respectively. The vertical (V =0) dashed line is a guide to the eye, highlighting the relative shifts of the band edges in the doped samples in manner typical of p-doped and n-doped semiconductors for the Aq-doped and Cu-doped nanocrystals, respectively. The inset shows an STM

image of a single (Ag-doped) OD

on which STS data were measured.



similar to the undoped QD, consistent with the optical measurements. However, the features in the scanning tunneling spectroscopy (STS) spectra are washed out, suggesting that indeed Au has entered the QD, perturbing the pristine level structure. More notable changes are seen for both the Cu and Ag cases (Fig. 3, upper panel), where band-tailing into the gap and the emergence of in-gap states in regions covering nearly 40% of the gap region are observed. In particular, in the Cu case, a shoulder on a tail-state structure is seen at bias values just below the  $1S_e$ doublet (which is remarkably preserved). Additionally, the doublet is superimposed on a notable rising background that increases to the region of the  $1P_{\rm e}$  peaks that are not well resolved (fig. S13). For the Ag-doped QDs, there is pronounced broadening and merging of features on the positive-bias side, and on the negative-bias side a background signal develops.

A clear result of doping in bulk semiconductors is the shift of the Fermi level, which for n-type doping is close to the conduction band, and conversely shifts to a lower energy close to the valence band for p-type impurities. Remarkably, such shifts are clearly identified in the STS of the Cu- and Ag-doped QDs, as measured by the positions of the band edges relative to zero bias. Whereas the Fermi energy for the undoped case, as well as the Au-doped case, is nearly centered, in the Cu-doped case the onset of the conduction band states nearly merges with the Fermi energy, consistent with n-type doping. In contrast, for the Ag-doped case, the Fermi level is much closer to the onset of the valence band states, signifying p-type doping in this case. Considering that the only difference between the samples is the type of impurity atoms, and that the measurements are carried out under the same conditions, surface ligand effects or environmental influences on the Fermi energy shifts (4, 9, 11, 28) can be ruled out.

Chemical considerations for the doping of InAs with the different metal atom impurities can help to clarify these observations (fig. S17). Cu can have a formal oxidation state of either +1 or +2. Moreover, its ionic radius is the smallest of the three impurities and therefore may be accommodated in interstitial sites within the InAs lattice (29). In such a case, one can expect that the Cu will partly donate its valence electrons to the QD, leading to n-type doping, consistent with the shift in the Fermi energy observed by STS. The incorporation of multiple impurities is expected to lead to the development of closely spaced impurity states, akin to the impurity band formed in the bulk (20). This band forms asymmetrically because of the disordered arrangement of the impurities in the QD, surpassing the energy of the 1S<sub>e</sub> QD state. The observed rising background in the STS curve signifies the presence of such an impurity band. This is a direct indication of the substantial modification of the DOS induced by the impurities in small, heavily doped QDs. Revisiting the observed blue shift in the absorption, this is in line with the filling of the conduction and impurity-band levels in heavily n-type doped QDs, leading to a Moss-Burstein blue shift in the absorption spectrum and minor shifts in the emission (Fig. 2). Furthermore, the addition of impurity levels explains the negligible bleach in the absorption with doping, in contrast to remote surface doping in which QD state filling by the contributed charges leads to a bleach (9-11).

Ag has a large radius and is considered to be a substitutional impurity in III-V semiconductors (30). The replacement of an In atom, which possesses three valence electrons, with a Ag atom, which has only one valence electron, leads to an electron deficiency in the bonding orbitals, causing p-type doping. This is reflected in the shift of the Fermi level, as seen in the STS data (Fig. 3, red trace). In this case, the rising background in the spectrum at negative bias indicates the formation of an impurity band near the valence band. Because Ag has the largest ionic radius of the three impurities, it distorts the crystal structure more than the others; this results in bandtailing analogous to the Urbach tail known for heavily doped bulk semiconductors, and leads to the red shifts observed in the absorption onset as well as the emission (Fig. 2). Au may adopt a +3 valence state, which makes it isovalent with In, and hence doping is not expected to lead to the introduction of charge carriers. Moreover, its size is comparable to that of In (table S1), allowing for substitutional doping without substantial

lattice distortions. These features of Au are consistent with the absence of large shifts in absorption, emission, and Fermi energy, as observed in both optical and tunneling spectra.

We also modeled the effects of electronic doping and structural disorder on the electronic properties of strongly confined impurity dopants in QDs. Starting with electronic effects, two models representing two limiting cases of doping were developed (26). The starting point for both models is based on the hydrogenic-like impurity model (22-24). In the first limit ("Z-model," Fig. 1B), we assume weak localization of the impurity states represented as a single central multivalent impurity. In the other limit, impurity electrons are sufficiently localized, to an extent much greater than in bulk (8), such that a singleelectron tight binding (TB) treatment where each impurity contributes a single electron was applied. In Fig. 4A, we show the impurity DOS for n-type doping of two QD sizes for the TB model. For small number of impurities (e.g., N = 5), a peak in the DOS is observed below the QD level  $(1S_e)$ . As the number of impurities increases, an impurity band develops asymmetrically around the QD level, pushing the Fermi energy toward the conduction band. The emerging impurity band develops a tail that extends into the gap, consistent with the STS data for the Cu case.

In Fig. 4B we show TB estimations for the shifts in the absorption spectrum as a function of the QD radius for various doping levels. The single impurity limit is the solution of a finitebarrier confined hydrogenic impurity, and nearly scales as  $R^{-1}$ . In this case, for both types of doping, a red shift is calculated. Although the confined energy levels of the impurity and the QD depend strongly on the effective mass  $(m_{e,h}^*)$ , the spectral shifts, which depend on the differences between the impurity and electron/hole levels, only depend weakly on  $m_{\rm e,h}^*$  (Fig. 4B). Indeed, to lowest order in the Coulomb interaction, these differences are given by the expectation value of the electrostatic energy. As the number of impurity atoms increases, we find a nonmonotonic dependence of the spectral shifts with QD size. This reflects the transition of the impurity DOS from the gap region into the conduction band.

The onset of the blue shift and its magnitude depend on the model parameters (Fig. 4C). At low impurity concentrations, a red shift is always observed, consistent with the single hydrogenic impurity limit. A turnover from negative to positive shift is observed with increasing impurity density, depending on the degree of impurity carrier localization, which is determined by the ratio of the range of impurity interactions a and QD size R. The regime at which a blue shift is observed sets in earlier as a/R increases. Density

functional theory calculations (31) for single impurities in QDs suggest  $a/R \approx 1/3$ , implying a narrow regime of red shift before a blue shift sets in. This is qualitatively consistent with the experimental observations shown in Fig. 4D for Cu, where a red shift is absent, suggesting that a < R. Moreover, the size dependence of the blue shift, which decreases with increasing R, is consistent with the R-dependence shown in Fig. 4C for the theory. The theory predicts that the shift will eventually reach a plateau, which is not observed experimentally.

The asymmetry in the shift (Fig. 4C) is directly correlated with the magnitude of the hopping term, γ. The case shown in Fig. 4C is for  $\gamma = 5\epsilon$  (where  $\epsilon$  is the single-impurity energy taken from the hydrogenic model), where the blue shift is noticeably larger. When  $\gamma = \varepsilon$ , one observes a symmetric shift around the QD level (fig. S22). Also shown in Fig. 4C are the results of the Z-model, yielding an opposite behavior (inconsistent with the experiments), where a blue shift is observed for low doping levels, turning to a red shift as the doping level increases. These fundamental differences between the Z- and TBmodels suggest that confinement leads to localization, consistent with previous theoretical work on single dopants (8).

An additional important mechanism of electronic level modification in the regime of heavily

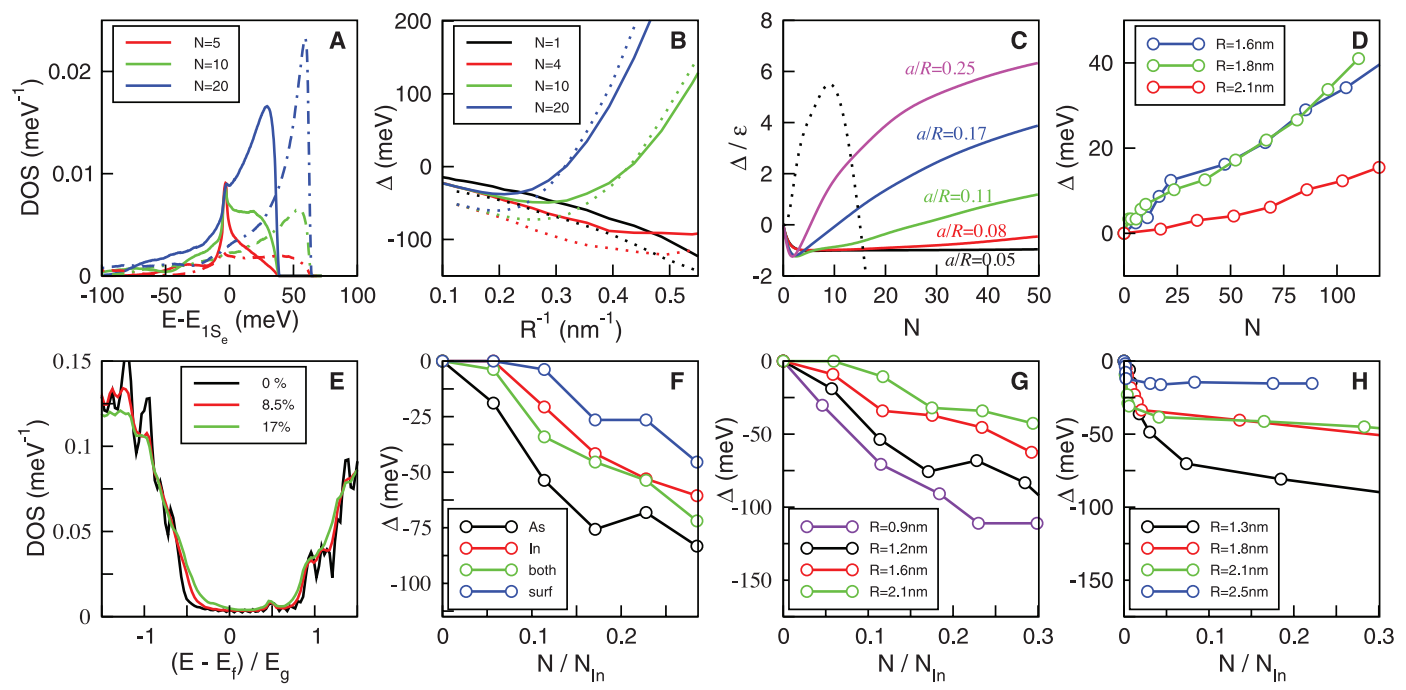


**Fig. 4.** The effect of doping on the electronic structure of nanocrystals. (A-D) Impurity band formation. (**A**) The impurity DOS from the TB model (a = 0.4 nm) for different levels of n-type doping for R = 2 nm (solid curves) and R = 1.3 nm (dotted-dashed curves). (**B**) The spectral shifts as a function of the inverse QD size for n-type (solid curves) and p-type (dotted curves) doping for different numbers of impurities. The InAs levels were calculated from an effective mass model. The impurity levels were calculated from the TB model with a = 0.4 nm. (**C**) Spectral shifts for n-type doping, as a function of the number of impurities N in units of the onsite energy in the tight binding model,  $\varepsilon$ , for several levels of

localization (a/R). Dashed curve is the result of the Z-model. (**D**) Experimental spectral shifts for Cu doping as a function of N for several QD sizes. (**E** to **H**) Band tailing in doped nanocrystals. (**E**) DOS of an  $\ln_{140}As_{141}$  QD for three levels of doping, expressed as a percentage of displaced In atoms. (**F**) Shifts in gap as a function of N relative to the number of In atoms ( $N_{In}$ ) in the NC for different ways of introducing structural disorder. (**G**) Calculated shifts induced by bandtailing for several QD sizes. (**H**) Measured spectral shifts for Ag-doped QDs for several QD sizes. We used a normal distribution to induce disorder with a width that is 10% the In-As bond length [see (26) for more details on the calculations].

doped semiconductors relates to distortions of the crystal structure by the dopants leading to bandtailing and a red shift of the gap. To address the role of band-tailing we employed an atomistic treatment of the electronic structure of the QD, where disorder was introduced by randomly displacing In or As atoms (26). Band-tailing occurs mainly for the valence band edge as evident from the DOS shown in Fig. 4E for different impurity numbers. This results from the heavier effective mass and the denser level structure of the valence band, compared to the light effective mass of the highly delocalized electron. From the DOS we estimate the shifts in the band gaps induced by disorder as shown in Fig. 4F. Tailing occurs for distortions to the In atoms, As atoms, both atoms or only surface atoms. The band gap decreases for higher dopant concentrations. Note that the As distortions lead to larger shifts, consistent with its larger ionic radii.

In Fig. 4, G and H, we show the calculated and measured shifts (for Ag impurities) for several QD sizes as a function of the dopant concentration, respectively. The striking similarities between the theory and experiments suggest that the spectral shifts observed in Ag, unlike the case of Cu, are dominated by band-tailing, although clearly in both cases there is an interplay between band tailing and the impurity band formation. Both theory and experiments show a rapid increase in the magnitude of the shift, reaching a plateau at high dopant concentrations. The increase in the shift depends on the level of disorder induced by each dopant. Furthermore, the shifts decrease with increasing QD size in both cases. We note that in Cu, although a contribution of band-tailing is also possible, the band-filling effect discussed above dominates, leading to the blue shift in that case.

Doping semiconductor NCs with metal impurities provides further means to control their optical and electronic properties. We developed a synthesis for n- and p-type doped InAs NCs by introducing Cu and Ag impurities, respectively. Cu-doped particles showed a blue shift in the absorption with only small bleaching. This is in line with the increased DOS, which results from the addition of new impurity levels that develop into an impurity band, and their partial filling with electrons from interstitial Cu impurities. Correspondingly, the STS measurements show a shift in the Fermi energy to near the conduction band edge, and the development of a confined impurity band. This behavior was rationalized by a TB model, and its size dependence indicates that the confinement leads to localization of the impurity states in small NCs. Conversely, STS measurements of Ag-doped NCs led to a shift of the Fermi energy toward the valence band, proving p-type doping. This was accompanied by a red shift of both absorption and emission peaks, attributed to bandtailing effects analogous to the Urbach tail, in line with Ag adopting substitutional sites. The magnitude and size dependence of the band

narrowing agree with atomistic electronic structure calculations incorporating structural disorder induced by the dopants. Interestingly, introduction of Au impurities as a substitutional dopant, although broadening the STS spectra, maintains the position of the Fermi level and does not lead to spectral shifts, in line with its isovalent nature with In. The controlled ability to synthesize n- and p-type doped NCs, along with better understanding of the heavily doped impurity regime in colloidal QDs, opens avenues for diverse electronic and optoelectronic devices.

#### References and Notes

- 1. S. M. Sze, *Physics of Semiconductor Devices* (Wiley-Interscience, New York, ed. 2, 1981).
- S. Coe, W.-K. Woo, M. Bawendi, V. Bulović, *Nature* 420, 800 (2002).
- I. Gur, N. A. Fromer, M. L. Geier, A. P. Alivisatos, Science 310, 462 (2005).
- 4. D. V. Talapin, C. B. Murray, Science 310, 86 (2005).
- D. J. Norris, A. L. Efros, S. C. Erwin, Science 319, 1776 (2008).
- 6. D. Turnbull, J. Appl. Phys. 21, 1022 (1950).
- G. M. Dalpian, J. R. Chelikowsky, *Phys. Rev. Lett.* 96, 226802 (2006).
- T. L. Chan, M. L. Tiago, E. Kaxiras, J. R. Chelikowsky, Nano Lett. 8, 596 (2008).
- 9. M. Shim, P. Guyot-Sionnest, Nature 407, 981 (2000).
- C. Wang, M. Shim, P. Guyot-Sionnest, Science 291, 2390 (2001).
- D. Yu, C. J. Wang, P. Guyot-Sionnest, Science 300, 1277 (2003).
- N. Pradhan, D. Goorskey, J. Thessing, X. Peng, J. Am. Chem. Soc. 127, 17586 (2005).
- 13. R. N. Bhargava, D. Gallagher, X. Hong, A. Nurmikko, *Phys. Rev. Lett.* **72**, 416 (1994).
- C. A. Stowell, R. J. Wiacek, A. E. Saunders, B. A. Korgel, Nano Lett. 3, 1441 (2003).
- 15. S. C. Erwin et al., Nature **436**, 91 (2005).
- Y. Yang, O. Chen, A. Angerhofer, Y. C. Cao, J. Am. Chem. Soc. 128, 12428 (2006).
- C. Tuinenga, J. Jasinski, T. Iwamoto, V. Chikan, ACS Nano
  1411 (2008).
- 18. S. Roy et al., J. Phys. Chem. C 113, 13008 (2009).

- R. Xie, X. Peng, J. Am. Chem. Soc. 131, 10645 (2009).
- R. A. Abram, G. J. Rees, B. L. H. Wilson, Adv. Phys. 27, 799 (1978).
- 21. J. Tauc, Ed., Amorphous and Liquid Semiconductors (Plenum. London. 1976).
- N. Porras-Montenegro, S. T. Perez-Merchancano, A. Latge, J. Appl. Phys. 74, 7624 (1993).
- S.-S. Li, J.-B. Xia, J. Appl. Phys. 101, 093716 (2007).
- M. Barati, G. Rezaei, M. R. K. Vahdani, *Phys. Status Solidi* 244, 2605 (2007) (b).
- T. Mokari, A. Aharoni, I. Popov, U. Banin, *Angew. Chem. Int. Ed.* 45, 8001 (2006).
- 26. See supporting material on Science Online.
- U. Banin, O. Millo, Annu. Rev. Phys. Chem. 54, 465 (2003).
- K. S. Leschkies, M. S. Kang, E. S. Aydil, D. J. Norris, I. Phys. Chem. C 114, 9988 (2010).
- 29. J. Dixon, D. Enright, J. Appl. Phys. 30, 753 (1959).
- 30. B. Tuck, P. R. Jay, J. Phys. D 11, 1413 (1978).
- D. V. Melnikov, J. R. Chelikowsky, *Phys. Rev. Lett.* 92, 046802 (2004).
- 32. We thank the staff of the Unit for Nanocharacterization of the Center for Nanoscience and Nanotechnology in the Hebrew University, Jerusalem, headed by I. Popov, as well as V. Gutkin for help in the XPS studies. Supported by a grant from the European Research Council under the European Community's Seventh Framework Programme (FP7/2007-2013)/ERC grant agreement 203413 (U.B.); the Israel Science Foundation (O.M.); Seventh Framework Programme Marie Curie International Outgoing Fellowships for Career Development project Hierarchical Junction Solar Cells (E.R.); the Harry de Jur Chair in Applied Science (O.M.); the Alfred and Erica Larisch Memorial Chair (U.B.): an Azrieli Foundation fellowship (G.C.); and the Centre for Scientific Absorption, Ministry of Absorption, State of Israel (D.M.).

#### Supporting Online Material

www.sciencemag.org/cgi/content/full/332/6025/77/DC1 Materials and Methods Figs S1 to S24

Table S1 References

10 August 2010; accepted 10 February 2011 10.1126/science.1196321

# **Electrochemically Mediated Atom Transfer Radical Polymerization**

Andrew J. D. Magenau, Nicholas C. Strandwitz, Armando Gennaro, Krzysztof Matyjaszewski \*\*

Atom transfer radical polymerization is a versatile technique for exerting precise control over polymer molecular weights, molecular weight distributions, and complex architectures. Here, we show that an externally applied electrochemical potential can reversibly activate the copper catalyst for this process by a one-electron reduction of an initially added air-stable cupric species (Cu<sup>II</sup>/Ligand). Modulation of polymerization kinetics is thereby tunable in real time by varying the magnitude of applied potential. Application of multistep intermittent potentials successfully triggers initiation of polymerization and subsequently toggles the polymerization between dormant and active states in a living manner. Catalyst concentrations down to 50 parts per million are demonstrated to maintain polymerization control manifested in linear first-order kinetics, a linear increase in polymer molecular weight with monomer conversion, and narrow polymer molecular weight distributions over a range of applied potentials.

iving polymerizations, introduced in 1956 by Szwarc (1), proceed in the absence of chain termination and chain transfer

events, while concurrently maintaining instantaneous initiation and uniform growth of each propagating species (2). Processes of this nature allow